miRNA-Signature of Irradiated Ptch1+/– Mouse Lens is Dependent on Genetic Background

Authors: Tanno, B., Babini, G., Leonardi, S., De Stefano, I., Merla, C., et al.

Source: Radiation Research, 197(1) : 22-35

Published By: Radiation Research Society

URL: https://doi.org/10.1667/RADE-20-00245.1

RADIATION RESEARCH **197**, 22–35 (2022)
0033-7587/22 $15.00

DOI: 10.1667/RADE-20-00245.1

miRNA-Signature of Irradiated *Ptch1*$^{+/-}$ Mouse Lens is Dependent on Genetic Background

B. Tanno,[a] G. Babini,[b,c] S. Leonardi,[a] I. De Stefano,[a] C. Merla,[a] F. Novelli,[a] F. Antonelli,[a] A. Casciati,[a] M. Tanori,[a] E. Pasquali,[a] P. Giardullo,[a] LDLensRad Consortium,[1] S. Pazzaglia[a,2] and M. Mancuso[a,2]

[a] *Laboratory of Biomedical Technologies, Agenzia Nazionale per le Nuove Tecnologie, l'Energia e lo Sviluppo Economico Sostenibile (ENEA), Rome, Italy;* [b] *Department of Physics, University of Pavia, Pavia, Italy; and* [c] *Department of Woman and Child Health and Public Health, Fondazione Policlinico A. Gemelli, Istituto di Ricovero e Cura a Carattere Scientifico (IRCCS), Rome, Italy*

Tanno, B., Babini, G., Leonardi, S., De Stefano, I., Merla, C., Novelli, F., Antonelli, F., Casciati, A., Tanori, M., Pasquali, E., Giardullo, P., LDLensRad Consortium, Pazzaglia, S. and Mancuso, M. miRNA-Signature of Irradiated *Ptch1*$^{+/-}$ Mouse Lens is Dependent on Genetic Background. *Radiat. Res*. 197, 22–35 (2022).

One harmful long-term effect of ionizing radiation is cataract development. Recent studies have been focused on elucidating the mechanistic pathways involved in this pathogenesis. Since accumulating evidence has established a role of microRNAs in ocular diseases, including cataract, the goal of this work was to determine the microRNA signature of the mouse lens, at short time periods postirradiation, to understand the mechanisms related to radio-induced cataractogenesis. To evaluate the differences in the microRNA profiles, 10-week-old *Patched1* heterozygous (*Ptch1*$^{+/-}$) mice, bred onto two different genetic backgrounds (CD1 and C57Bl/6J), received whole-body 2 Gy γ-ray irradiation, and 24 h later lenses were collected. Next-generation sequencing and bioinformatics analysis revealed that genetic background markedly influenced the list of the deregulated microRNAs and the mainly predicted perturbed biological functions of 2 Gy irradiated *Ptch1*$^{+/-}$ mouse lenses. We identified a subset of microRNAs with a contra-regulated expression between strains, with a key role in regulating Toll-like receptor (TLR)-signaling pathways. Furthermore, a detailed analysis of miRNome data showed a completely different DNA damage response in mouse lenses 24 h postirradiation, mainly mediated by a marked upregulation of p53 signaling in *Ptch1*$^{+/-}$/C57Bl/6J lenses that was not detected on a CD1 background. We propose a strict interplay between p53 and TLR signaling in *Ptch1*$^{+/-}$/C57Bl/6J lenses shortly after irradiation that could explain both the resistance of this strain to developing lens opacities and the susceptibility of CD1 background to radiation-induced cataractogenesis through activation of epithelial-mesenchymal transition.

INTRODUCTION

MicroRNAs (miRNAs), short non-coding RNA sequences of ~22 nucleotides, are a large family of post-transcriptional negative regulators of gene expression on the mRNA level. A single miRNA can regulate even hundreds of transcripts, and a single transcript is influenced by different miRNAs (*1*). It has been postulated that mature miRNAs control transcription of more than 60% of all protein-coding genes, regulating several biological processes (*2*). The study of miRNA-target interactions is an emerging area of research, due also to the causal relationship between miRNAs and disease development. Since the first release of miRTarBase in 2011, experimentally validated miRNA-target interactions have been continuously accumulated for nearly 10 years and the latest release of this online resource (version 8.0) reports 479.340 curated miRNA-target interactions between 4.312 miRNAs and 23.426 target genes (*3*).

The key role of miRNAs has been recognized in different diseases, among which are cancers (*4*), cardiovascular (*5*), inflammatory (*6*), auto immune (*7*) and liver diseases (*8*), as well as skin fibrosis (*9*) and neurocognitive dysfunctions (*10*). Accumulating miRNA profiling studies have demonstrated that they are deregulated also in cataract (*11*). In a comparison of the central epithelium of transparent and age-related cataractous human lenses, significant differences were identified in miRNA expression profiles (*12*). Of note, it has also been suggested that deregulated miRNAs can contribute to age-related cataractogenesis by targeting the 3′ untranslated region and/or TATA-box region of oxidative

Editor's note. The online version of this article (DOI: https://doi.org/10.1667/RADE-20-00245.1) contains supplementary information that is available to all authorized users.

[1] For the LDLensRad Consortium: E. Ainsbury, M. Ahmadi, T. Azizova, F. Antonelli, G. Babini, S. Barnard, C. Dalke, L. Dauer, I. De Stefano, J. Dynlacht, L. Garrett, J. Graw, N. Hamada, S. M. Hölter, M. Jarrin, M. Kadhim, A. Kalligeraki, S. Kunze, S. Leonardi, M. Mancuso, R. McCarron, J. Moquet, D. Pawliczek, S. Pazzaglia, R. Quinlan, A. Saran, R. Tanner, B. Tanno, M. Ung and A. Uwineza.

[2] Address for correspondence: M. Mancuso or S. Pazzaglia: Laboratory of Biomedical Technologies, ENEA Casaccia Research Centre, 00123 Rome, Italy; email: mariateresa.mancuso@enea.it; simonetta.pazzaglia@enea.it.

stress-related genes, resulting in elevation of pro-oxidative genes and inhibition of anti-oxidative genes (*13*).

It is well known that reactive oxygen species (ROS) can be endogenously produced by the normal cellular metabolism or exogenously originated by exposure to ionizing radiation, resulting in a high local production of ROS attributable to chemical interactions between high-energy electrons, photons, and the molecular targets of oxygen and water within cells (*14*). Radiation exposure is a recognized risk factor for cataract (*15*) and, currently, the International Commission on Radiological Protection assumes that the lens response to radiation is a deterministic effect/tissue reaction, with a dose threshold and no dose-rate effect (*16*). Although the correlation between radiation exposure and cataract is widely documented in epidemiological (*17, 18*), experimental *in vitro* and *in vivo* studies (*18–22*) and, more recently, by developing an *in silico* model useful to predict the risk for radiation-induced cataractogenesis (*23*), the involved mechanistic pathways are not elucidated in depth.

In an attempt to bridge this gap, we took advantage of *Patched1* heterozygous (*Ptch1*$^{+/-}$) mice, characterized by activation of the Sonic hedgehog (Shh) pathway, a molecular signaling that controls cell proliferation and cell fate during embryogenesis such as the maintenance of the stem cell compartment in adult tissues (*24*). Shh has been recognized to have a role in mouse lens development (*25*) and results of our previously published work have clearly demonstrated a specific role of the *Ptch1* gene in the maintenance of lens integrity with or without exogenous damage, validating the *Ptch1*$^{+/-}$ mice as a highly sensitive model of radiation-induced cataracts when radiation is delivered during the early stage of postnatal lens development (*22, 26*).

The goal of this study was to determine whether miRNome alterations could play a role in radiation-induced cataractogenesis by causing impairments of proper lens maintenance and their dependence on genetic background. To this aim, we analyzed miRNA expression in *Ptch1*$^{+/-}$ mouse lenses of CD1 and C57Bl/6J mice, γ-ray irradiated at 2 Gy (dose rate 0.3 Gy/min) at 24 h postirradiation, to mitigate the myriad of interactions among DNA damage response (DDR) components and miRNAs. We identified a set of miRNAs, modulated by radiation, controlling different biological functions and its expression was altered in a completely different way in the two genetic backgrounds. In addition, a more focused analysis of the DDR predicted genes, based on the deregulated set of miRNAs, showed a marked activation of p53 signaling in C57Bl/6J mouse lenses, which could be protective against the detrimental effect of radiation on the lens.

MATERIALS AND METHODS

Mice Irradiation and Dosimetry

Mice lacking one *Ptch1* allele were bred on CD1 (named *Ptch1*$^{+/-}$/CD1 throughout the text) or C57Bl/6J (*Ptch1*$^{+/-}$/B6) background and genotyped as described elsewhere (*27*). At 10 weeks of age, a total of 104 mice, equally distributed between sexes and genotypes. Mice were either sham irradiated (n = 52) or irradiated (n = 52) at the Italian National Institute of Ionizing Radiation Metrology (ENEA-INMRI), using the irradiation facility currently used for calibration of radiotherapy dosimeters. The beam used for the calibration was a horizontal ^{60}Co beam, with a field size of 10 × 10 cm at 100-cm distance from the source; the dose rate was 0.16 Gy/min as determined using a reference ionization chamber calibrated in terms of absorbed dose to water with traceability to the Italian primary standard of absorbed dose. Thus, to deliver 2 Gy at a dose rate of 0.3 Gy/min, the source distance was varied at 74.1 cm. Mice were irradiated in a poly(methyl methacrylate) (PMMA) holder with 4-mm-thick walls, ensuring electronic equilibrium conditions. The PMMA holder was placed with its midpoint at the source distance realizing the required dose rate within ± 2%. The irradiation time t_{irr} to deliver the required absorbed dose was calculated as:

$$t_{irr} = \frac{D}{\dot{D}} - t_{err},$$

where D is the delivered dose, $\dot{D}$ is the actual dose rate during irradiation and t_{err} is the timer error.

The number of mice simultaneously irradiated was established to ensure a beam uniformity within 1% and was determined to be n = 1.

All mice were housed under conventional conditions with food and water available *ad libitum* and 12:12 h light-dark schedule. Sham-irradiated mice were subjected to all the manipulations heretofore described in the irradiation session.

This animal study was performed according to the European Community Council Directive 2010/63/EU, approved by the local Ethical Committee for Animal Experiments of the ENEA, and authorized by the Italian Ministry of Health (no. 1233/2015-PR).

miRNome Analysis by Next-Generation Sequencing (NGS)

From unirradiated or 2 Gy irradiated *Ptch1*$^{+/-}$/CD1 and *Ptch1*$^{+/-}$/B6 mice as well as their wild-type (WT) counterparts (n = 4 for each experimental group), lenses were collected at 24 h postirradiation and total RNA was extracted using miRNeasy kit (QIAGEN, Milan, Italy) according to the manufacturer's instructions. RNA was quantified by optical density (OD) measurement using a NanoDrop spectrophotometer (Thermo Fisher Scientific Inc., Milan, Italy) and qualification was performed using the Agilent TapeStation 200 (Santa Clara, CA). The OD and RNA integrity number measurements for all RNA samples are provided in Supplementary Table S1 (https://doi.org/10.1667/RADE-20-00245.1.S1). RNA (100 ng) was thus converted into miRNA NGS libraries using NEBNEXT library generation kit (New England Biolabs® Inc., Beverly, MA) following manufacturer's instructions, thus sequenced data were analyzed according to Tanno *et al*. (*28*). Only statistically significant miRNAs ($P \leq 0.05$, log fold-change ≥ 0.7) were used for gene/miRNA enrichment analysis with Cytoscape plug-in ''ClueGo'' (version 2.1.7) and ''CluePedia'' (version 1.1.7) (*29*) with a validated miRTarBase SCORE > 0.6. Top 20 predicted target genes for each miRNA in the list were finally selected to identify the affected pathways and functions on the REACTOME database (https://reactome.org), considering a minimum number of genes into the pathway equal to 3 with a percentage not less than 4.

Identification of miRNAs Predicted Target Genes Involved in DNA Damage Repair (DDR) Pathways

Gene sets belonging to the main DDR pathways (HR, NHEJ, MMR, NER, BER and P53) were taken from the ''KEGG C2'' curated collection at the Molecular Signature Database (MSigDB) (https://bit.ly/3c9khiY). All miRNAs known to have predicted target genes among each gene of the six pathways were extracted by the ''miRDB - MicroRNA Target Prediction Database'' target mining function

(http://www.mirdb.org/mining.html). The following parameters have been considered for the query: 1. Exclude gene targets with less than 60 as target prediction score; 2. Exclude miRNAs with more than 2,000 predicted targets in genome; 3. Species: Mouse; 4. Include all miRNAs. *Ad hoc* implemented matching algorithm in statistical software R allowed identification of miRNAs (with predicted target genes in the DDR response) that were found to be differentially expressed in our comparisons. The identified miRNAs, their corresponding fold-changes, the predicted target genes, the predicted action (activation or inhibition, depending on the fold-change) and the corresponding DDR pathway were all structured in a table and imported in Cytoscape as networks.

Quantitative qPCR

Total RNA was isolated using RNeasy Mini Kit (QIAGEN, Milan, Italy) from lenses (n = 4) 24 h or 4 months postirradiation. After quantification by NanoDrop (Thermo Fisher Scientific), RNA (2 μg) was reverse transcribed using the High-Capacity cDNA Reverse Transcription Kit (Applied Biosystems®, Foster City, CA), and qPCR was performed with the StepOnePlus™ Real-Time PCR System (Applied Biosystems) using Power SYBR® Green PCR Master Mix (Applied Biosystems). Oligonucleotide primers used to evaluate gene expression are provided in Supplementary Table S2 (https://doi.org/10.1667/RADE-20-00245.1.S1). Reactions were performed in triplicate from each biological replicate. Relative gene expression was quantified using glyceraldehyde-3-phosphate dehydrogenase (*Gapdh*), β-*actin* and ribosomal protein L32 (*RPL32*) as housekeeping genes

miRNA analysis was performed using the TaqMan® miRNA Assay (Thermo Fisher Scientific) for hsa-miR-124, hsa-miR-34a and for U6 snRNA as housekeeping. The DDCt quantitative method was used to normalize expression of the reference gene and to calculate the relative expression levels of target genes.

Histology and Immunohistochemistry

Eyes (n = 20 per each genetic background) were collected from mice 4 months postirradiation (n = 10) and from their nonirradiated age-matched counterparts (n = 10), fixed in 10% buffered formalin and paraffin embedded. Sections (4 mm) were cut in a plane perpendicular to the anteroposterior eye axis and stained with hematoxylin and eosin (H&E) or immunostained with an antibody direct against N-cadherin (N-cad, polyclonal; Cell Signaling Technology® Inc., Danvers, MA) (1:200).

Western Blot Analysis

Proteins were extracted from lenses (n = 4) from mice 4 months postirradiation and from their nonirradiated age-matched counterparts using T-PER® Tissue Protein Extraction Reagent (Pierce Biotechnology, Rockford, IL) added with protease inhibitors. Proteins were separated on pre-cast gels (Bio-Rad® Laboratories, Hercules, CA) and transferred onto a polyvinylidene fluoride (PVDF) membrane (pore size 0.45 mm; Immobilion®-P, Millipore, Burlington, MA). Filters were blocked with 3% bovine serum albumin (BSA) dissolved in Tris-buffered saline (TBS) with 0.05% Tween®-20 (TBS-T) for 0.5 h at room temperature. Membranes were then incubated at 4°C overnight with anti-Smad3 phospho S423/S425 (Abcam, Cambridge, UK; 1:1,000) and β-actin (Sigma-Aldrich ® LLC, St. Louis, MO). Specific proteins were visualized using ImageQuant™ LAS 500 (GE Healthcare Europe GmbH, Milan, Italy) and densitometric analysis was performed using ImageJ version 1.52v software (https://imagej.it.softonic.com; Softnonic Corp., Barcelona, Spain).

Statistical Analysis

All the end points investigated (i.e., qPCR, Western blotting) are reported as means ± standard error of the mean (SEM), and two-tailed Student's *t* test was used for determining the statistical difference between the analyzed groups. $P \leq 0.05$ was considered statistically significant. Analyses were performed using GraphPad Prism version 6.0 (San Diego, CA) for Microsoft® Windows® (Redmond, WA).

RESULTS

Differentially Expressed miRNAs in Irradiated Lenses of Ptch1$^{+/-}$/CD1 and Ptch1$^{+/-}$/B6 mice and their WT Counterparts

To elucidate the role of the genetic background in radiation-induced cataractogenesis, we first analyzed the modulation of miRNAs dependent on radiation, comparing 2 Gy irradiated *Ptch1*$^{+/-}$/CD1 mouse lenses to nonirradiated ones. Results reported in Table 1 show 40 statistically differentially expressed miRNAs ($P < 0.05$); of these, 38 were upregulated while the remaining two were downregulated. Pathway analysis (Fig. 1B and C), obtained after selection of the top 20 genes with a validated miRTarBase value > 0.6 (Fig. 1A) and querying the REACTOME database, predicted the deregulation of interferon (IFN)-mediated response and, importantly, the activation of an innate immune response through the Toll-like receptor cascades (TLRs), belonging to a broad range of sensors, termed pattern recognition receptors (*30*). This network was mostly predicted by a subset of miRNAs, i.e., mmu-miR-490-3p, mmu-miR-124-3p, mmu-miR-145a-5p, mmu-miR-143-3p, mmu-miR-150-5p, mmu-miR-199-5p and mmu-miR-138-5p. Other identified pathways are mainly involved in signaling by tyrosine kinase receptors (PDGF, SCF-KIT MET and PTK6) and non-tyrosine kinase receptors.

Results obtained after miRNome analysis of 2 Gy irradiated *Ptch1*$^{+/-}$/B6 mouse lenses are shown in Table 2. By comparing with the baseline levels of miRNAs expressed in nonirradiated lenses, we obtained 24 statistically significant deregulated miRNAs, most of them downregulated (16/24). The predicted pathways identified by the deregulated miRNAs (Fig. 2) converged on the deactivation of the β-catenin trans-activating complex (mmu-miR-690 and mmu-miR-143-3p), and, to a greater extent, on the deregulation of cyclin D-associated events in G_1 cell cycle phase (mmu-miR-145a-5p and mmu-miR-391-5p), suggesting a deregulation of cell cycle progression (*31*).

Notably, predicted pathways (Supplementary Fig. S1A; https://doi.org/10.1667/RADE-20-00245.1.S1) obtained from the 55 (51 up- and 4 downregulated) statistically differentially expressed miRNAs ($P < 0.05$), found comparing 2 Gy irradiated to nonirradiated CD1 mouse lenses, clearly showed the activation of almost all pathways listed in Fig. 1C. Alternatively, among the very low number of statistically differentially expressed miRNAs (n = 13, $P < 0.05$, all downregulated) obtained from C57Bl/6J mouse lenses (2 Gy vs. nonirradiated), the only predicted pathway was the mTOR signaling (Supplementary Fig. S1B), suggesting again a deregulation of cell cycle progression.

TABLE 1
Differentially Expressed miRNAs in 2 Gy Irradiated (0.3 Gy/min) vs. Sham-Irradiated *Ptch1*$^{+/-}$/CD1 Mouse Lenses

miRNA	logFC[a]	logCPM[b]	*P* value	FDR[c]
mmu-miR-3473b	2.02	2.55	1.00×10^{-6}	2.00×10^{-4}
mmu-miR-690	1.84	3.56	2.00×10^{-6}	5.00×10^{-4}
mmu-miR-3968	1.56	3.89	4.80×10^{-5}	6.50×10^{-3}
mmu-miR-150-5p	1.33	7.07	3.23×10^{-4}	3.31×10^{-2}
mmu-miR-145a-5p	1.26	7.84	6.51×10^{-4}	5.34×10^{-2}
mmu-miR-143-3p	1.16	11.74	1.55×10^{-3}	1.06×10^{-2}
mmu-miR-211-3p	1.08	5.12	3.75×10^{-3}	2.02×10^{-2}
mmu-miR-145a-3p	1.14	4.47	3.95×10^{-3}	2.02×10^{-1}
mmu-miR-129-2-3p	0.98	7.11	7.44×10^{-3}	3.09×10^{-1}
mmu-miR-873a-5p	0.98	5.08	8.32×10^{-3}	3.09×10^{-1}
mmu-miR-143-5p	1.02	4.94	9.58×10^{-3}	3.09×10^{-1}
mmu-miR-5100	–1.00	2.67	9.84×10^{-3}	3.09×10^{-1}
mmu-miR-127-3p	0.95	7.06	9.99×10^{-3}	3.09×10^{-1}
mmu-miR-199a-5p	0.94	6.47	1.10×10^{-2}	3.09×10^{-1}
mmu-miR-383-5p	0.96	3.84	1.13×10^{-2}	3.09×10^{-1}
mmu-miR-490-3p	1.04	2.72	1.21×10^{-2}	3.09×10^{-1}
mmu-miR-124-3p	0.90	12.97	1.39×10^{-2}	3.26×10^{-1}
mmu-miR-1249-3p	0.93	3.81	1.50×10^{-2}	3.26×10^{-1}
mmu-miR-760-3p	0.94	3.66	1.51×10^{-2}	3.26×10^{-1}
mmu-miR-668-3p	0.91	3.53	1.82×10^{-2}	3.46×10^{-1}
mmu-miR-132-3p	0.86	7.87	1.84×10^{-2}	3.46×10^{-1}
mmu-miR-129-5p	0.86	9.10	1.86×10^{-2}	3.46×10^{-1}
mmu-miR-873a-3p	0.96	2.72	1.95×10^{-2}	3.46×10^{-1}
mmu-miR-199b-5p	0.86	5.76	2.03×10^{-2}	3.46×10^{-1}
mmu-miR-3099-3p	0.84	5.73	2.27×10^{-2}	3.73×10^{-1}
mmu-miR-96-5p	0.80	14.19	2.76×10^{-2}	4.27×10^{-1}
mmu-miR-18a-5p	–0.81	4.69	2.92×10^{-2}	4.27×10^{-1}
mmu-miR-485-5p	0.85	3.58	2.97×10^{-2}	4.27×10^{-1}
mmu-miR-485-3p	0.81	4.70	3.02×10^{-2}	4.27×10^{-1}
mmu-miR-217-5p	0.86	2.91	3.31×10^{-2}	4.40×10^{-1}
mmu-miR-190b-3p	0.86	2.95	3.37×10^{-2}	4.40×10^{-1}
mmu-miR-466q	0.89	2.30	3.43×10^{-2}	4.40×10^{-1}
mmu-miR-135b-5p	0.76	6.83	3.73×10^{-2}	4.54×10^{-1}
mmu-miR-183-5p	0.76	14.59	3.80×10^{-2}	4.54×10^{-1}
mmu-miR-138-5p	0.76	7.28	3.87×10^{-2}	4.53×10^{-1}
mmu-miR-451a	0.75	5.26	4.16×10^{-2}	4.74×10^{-1}
mmu-miR-323-3p	0.75	5.03	4.45×10^{-2}	4.80×10^{-1}
mmu-miR-434-3p	0.73	8.12	4.55×10^{-2}	4.80×10^{-1}
mmu-miR-183-3p	0.73	6.67	4.72×10^{-2}	4.80×10^{-1}
mmu-miR-187-3p	0.72	6.79	5.00×10^{-2}	4.80×10^{-1}

[a] FC = fold-change; [b] CPM = counts per million; [c] FDR = false discovery rate.

TABLE 2
Differentially Expressed miRNAs in 2 Gy Irradiated (0.3 Gy/min) vs. Sham-Irradiated *Ptch1*$^{+/-}$/B6 Mouse Lenses

miRNA	logFC[a]	logCPM[b]	*P* value	FDR[c]
mmu-miR-143-5p	–2.73	4.94	3.00×10^{-12}	1.00×10^{-9}
mmu-miR-145a-5p	–2.30	7.84	1.67×10^{-9}	3.43×10^{-7}
mmu-miR-143-3p	–2.22	11.74	5.08×10^{-9}	6.94×10^{-7}
mmu-miR-145a-3p	–2.16	4.47	2.20×10^{-8}	2.26×10^{-6}
mmu-miR-3473b	–1.54	2.55	1.63×10^{-4}	1.34×10^{-2}
mmu-miR-322-3p	1.30	4.24	7.33×10^{-4}	4.49×10^{-9}
mmu-miR-542-3p	1.26	5.41	7.66×10^{-4}	4.49×10^{-2}
mmu-miR-5100	–1.20	2.67	3.61×10^{-3}	1.81×10^{-1}
mmu-miR-665-3p	–1.14	2.76	3.99×10^{-3}	1.81×10^{-1}
mmu-miR-409-3p	–1.05	5.32	4.61×10^{-3}	1.89×10^{-1}
mmu-miR-351-5p	0.99	7.47	6.95×10^{-3}	2.59×10^{-1}
mmu-miR-490-3p	–1.03	2.72	7.64×10^{-3}	2.61×10^{-1}
mmu-miR-101c	–1.00	3.04	9.37×10^{-3}	2.96×10^{-1}
mmu-miR-540-3p	–0.97	3.28	1.26×10^{-2}	3.69×10^{-1}
mmu-miR-690	–0.96	3.56	1.36×10^{-2}	3.71×10^{-1}
mmu-miR-494-3p	–0.98	2.54	1.47×10^{-2}	3.76×10^{-1}
mmu-miR-144-5p	0.95	3.67	1.59×10^{-2}	3.84×10^{-1}
mmu-miR-322-5p	0.82	8.38	2.44×10^{-2}	5.31×10^{-1}
mmu-miR-1251-5p	–0.83	6.25	2.46×10^{-2}	5.31×10^{-1}
mmu-miR-503-5p	0.79	5.81	3.15×10^{-2}	6.25×10^{-1}
mmu-miR-3065-5p	–0.84	3.35	3.20×10^{-2}	6.25×10^{-1}
mmu-miR-802-5p	0.79	2.95	4.25×10^{-2}	7.79×10^{-1}
mmu-miR-503-3p	0.78	3.25	4.37×10^{-2}	7.79×10^{-1}
mmu-miR-299a-5p	–0.74	4.05	4.79×10^{-2}	8.18×10^{-1}

[a] FC = fold-change; [b] CPM = counts per million; [c] FDR = false discovery rate.

Intersection between Mouse Strains

To explore more in depth the radiation-dependent miRNA deregulation in the two different mouse genetic backgrounds, we intersected the statistically significant miRNAs perturbed in the lenses of *Ptch1*$^{+/-}$/CD1 and *Ptch1*$^{+/-}$/B6 after 2 Gy irradiation. As shown in Fig. 3A, the Venn diagram highlights 32 miRNAs exclusive for CD1 strain and 16 for B6, with 8 miRNAs in common, listed in Fig. 3B. Of note, 7 of the 8 common miRNAs were contra-regulated and only the mmu-miR-5100 was downregulated in both groups. Many of the contra-regulated miRNAs converged on the regulation of TLR cascades (*32*), indicating that, depending on the genetic background, inflammatory signaling can be differently restrained. To validate this result, we used qPCR to analyze the expression of the most relevant miRNA and genes involved in the TLR cascade. First, we analyzed the expression of miR-124-3p, which is known to negatively regulate multiple components of TLR signaling, including TLR6, MyD88, TNF-α and TNF receptor-associated factor 6 (*33*). This miRNA was one of the statistically differentially expressed miRNAs in 2 Gy irradiated *Ptch1*$^{+/-}$/CD1 mouse lenses (Table 1). Its expression was confirmed to be significantly upregulated after irradiation in *Ptch1*$^{+/-}$/CD1 lenses and, conversely, significantly reduced in 2 Gy irradiated *Ptch1*$^{+/-}$/B6 lenses compared to the respective nonirradiated conditions (Fig. 3C). As a next step, we analyzed the expression of key genes of TLR cascades, such as *TLR4*, *iRAK4* and *IkBa* and, as expected, they were significantly down- and upregulated in *Ptch1*$^{+/-}$/CD1 and *Ptch1*$^{+/-}$/B6 lenses after irradiation, respectively. (Fig. 3D–F).

miRNAs and DDR

To investigate the DDR in *Ptch1*$^{+/-}$/CD1 and *Ptch1*$^{+/-}$/B6 mouse lenses, we took advantage of the miRNome dataset designing an *ad hoc* focused analysis. Genes controlling the main DDR pathways (HR, NHEJ, MMR, NER, BER and p53) and miRNAs predicted to target their function were extracted from devoted databases and matched with the list of differentially expressed miRNAs resulting from our comparisons. These analyses led to the network visualizations shown in Fig. 4. In *Ptch1*$^{+/-}$/CD1 irradiated lenses, we

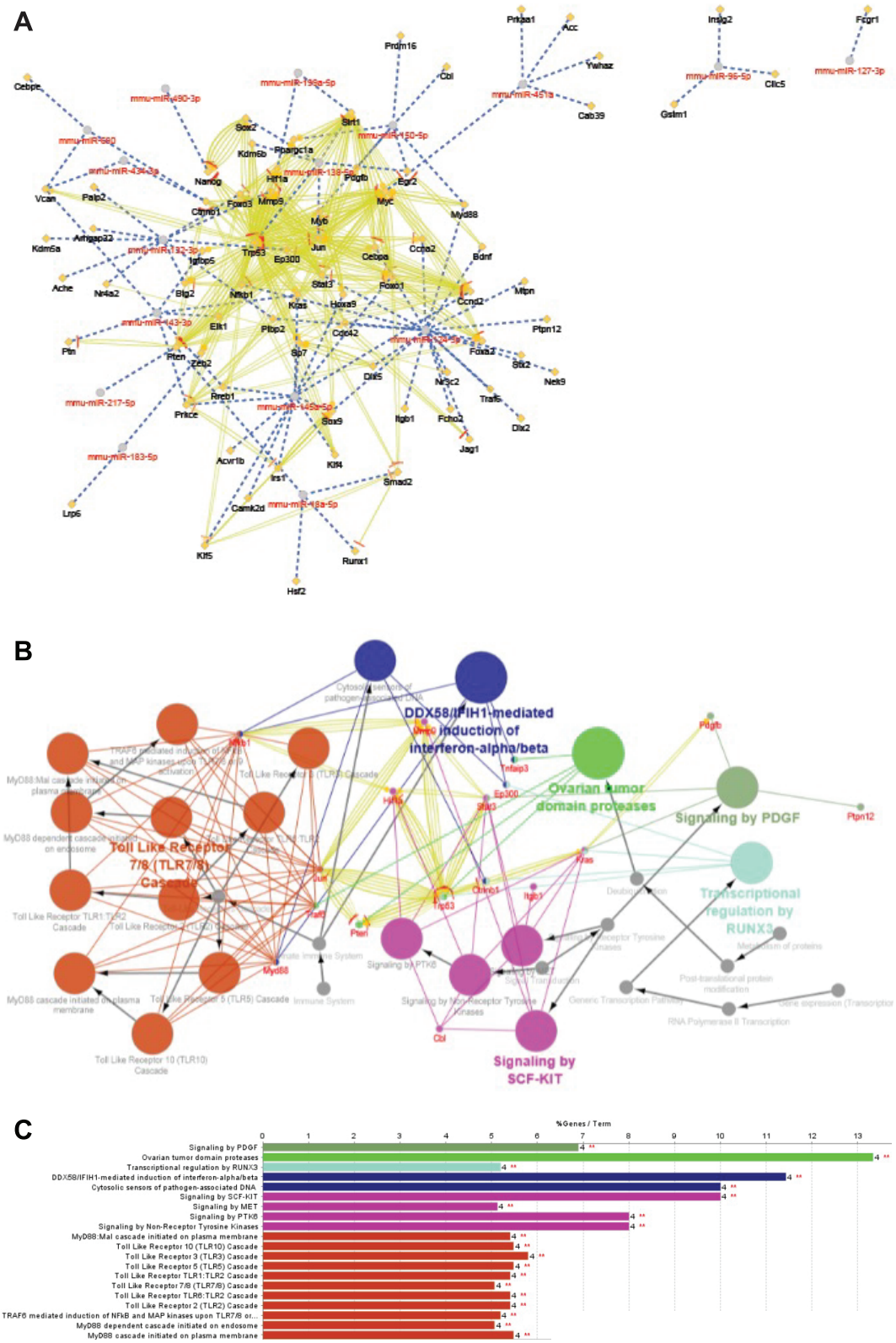

FIG. 1. *Ptch1*$^{+/-}$/CD1 mouse lenses: Pathway analysis. Panels A and B: miRNAs and their predicted target genes, and corresponding pathway analysis, respectively. Panel C: Histogram showing the most significant REACTOME pathways associated with the statistically significant miRNAs altered in 2 Gy irradiated vs. nonirradiated *Ptch1*$^{+/-}$/CD1 mouse lenses, listed in Table 1.

found a prominent downregulation of DDR-related genes, mostly due to the inhibition of the *p53* pathway (Fig. 4A). Conversely, in *Ptch1*$^{+/-}$/B6 mouse lenses, *p53* activation resulted in an overall upregulation of DDR pathways (Fig. 4B). To validate our results, we analyzed *p53* mRNA expression levels by qRT-PCR and, accordingly to the DDR-dedicated miRNome analysis, we found a statistically significant downregulation in *Ptch1*$^{+/-}$/CD1 lenses after irradiation and an opposite upregulation in *Ptch1*$^{+/-}$/B6 irradiated lenses.

To test whether p53 signaling was dysfunctional, we assessed the expression level of *p21*, a cyclin-dependent kinase inhibitor that is a major target of p53 activity and thus is associated with linking DNA damage to cell cycle arrest. Notably, *p21* was upregulated after irradiation in *Ptch1*$^{+/-}$/B6 lenses, while in *Ptch1*$^{+/-}$/CD1 no difference was found between irradiated and nonirradiated lenses (Fig. 5B).

We next evaluated the expression of miR-34a, a tumor suppressor miRNA transcriptionally activated by p53 (*34*) that is considered a critical mediator of its function. No difference in miR-34a expression was found between irradiated and nonirradiated lenses in *Ptch1*$^{+/-}$/CD1 mice 24 h after irradiation; instead, in the lenses of *Ptch1*$^{+/-}$/B6 mice, irradiation significantly increased miR-34a expression, strongly supporting the activation of p53 signaling cascade (Fig. 5C). miR-34 also plays a crucial role in controlling of epithelial-mesenchymal transition (EMT) through different mechanisms. In particular, miR-34a was shown to downregulate the expression of key genes in the TGF-β pathway, including TGF-β receptor 1 (TGF-βR1), Smad4 and Smad3 (*35*). Notably, there is extensive evidence on the critical role played by TGF-β in the initiation, development and persistence of radiation-induced fibrosis (*36*). Thus, we analyzed the expression level of *Smad3*, finding a significant decrease in its expression in *Ptch1*$^{+/-}$/B6 irradiated compared to nonirradiated lenses, but not in *Ptch1*$^{+/-}$/CD1 lenses (Fig. 5D).

On the complex, the DDR-dedicated miRNome analysis showed different responses of irradiated lenses in the two genetic backgrounds. Of note, the marked activation of p53 signaling in irradiated *Ptch1*$^{+/-}$/B6 mouse lenses can result in the suppression of EMT, a well-known trigger of radiation-induced cataractogenesis.

EMT Leads to Radiation-Induced Lens Opacity/ Cataractogenesis in Ptch1$^{+/-}$*/CD1 Lenses*

The canonical TGF-β signaling pathway uses Smad2 and/or Smad3 to transfer signals; Smad2/3 are, in fact, directly phosphorylated by Tgfbr1 and translocate to the nucleus to regulate gene transcription (*37*). To further elucidate the mechanisms of radiation-induced lens opacity/cataract, we assessed mRNA expression level of *Smad3* in mouse lenses 4 months postirradiation. At this age, irradiation did not increase *Smad3* expression in *Ptch1*$^{+/-}$/B6, while we found a significant increase in *Ptch1*$^{+/-}$/CD1 irradiated compared to nonirradiated lenses (Fig. 5E). We next quantified the expression level of phospho-Smad3 using Western blotting, finding a marked increase in *Ptch1*$^{+/-}$/CD1 irradiated lenses but no significant changes in *Ptch1*$^{+/-}$/B6 irradiated lenses (Fig. 5F and G). Morphological examination of nonirradiated mouse lenses showed no difference between *Ptch1*$^{+/-}$/CD1 and *Ptch1*$^{+/-}$/B6 mice (data not shown). Notably, 4 months postirradiation, exclusively *Ptch1*$^{+/-}$/CD1 lenses showed presence of abnormalities in both anterior (Fig. 5H–J) and posterior (Fig. 5K and L) poles of the lens. Mislocated nuclei (Fig. 5H) and presence of bladder cells (Fig. 5K and L) were commonly observed in the anterior and posterior poles, respectively. N-cad immunoreactivity (Fig. 5I) revealed in the lens epithelial cells (LECs) and the presence of plaques consisting of multilayered cells with spindle shaped features (Fig. 5L), reminiscent of fibroblastic morphology, clearly indicates that LECs have undergone an EMT aberrant culminating in anterior subcapsular cataract (ASC) development as previously reported elsewhere (*22, 38*).

DISCUSSION

The goal of this study was to improve the mechanistic understanding of individual susceptibility to radiation-induced cataract. In our experiments, the miRNome analysis showed different early radiation responses in the lens of *Ptch1*$^{+/-}$/B6 and *Ptch1*$^{+/-}$/CD1 mice, mainly involving TLR signaling and DDR, thus suggesting that radiation response in the lens is largely controlled by the genetic background. The miRNome pathway analysis identified the deregulation of TLRs pathway in irradiated *Ptch1*$^{+/-}$/CD1 lenses. Concordantly with miRNAs, the expression of key genes of *TLR* cascades (i.e., *TLR4*, *iRAK4* and *IkBa*) was significantly downregulated in *Ptch1*$^{+/-}$/CD1 and upregulated in *Ptch1*$^{+/-}$/B6 lenses after irradiation. In addition, DDR-focused miRNome analysis in *Ptch1*$^{+/-}$/B6 mouse lenses showed an exclusive marked activation of p53 signaling after irradiation that was opposed to the downregulation in *Ptch1*$^{+/-}$/CD1 irradiated lenses, pointing to important p53-driven genetic background-related differences in DNA repair mechanisms. Induction of p53 has been reported to repress cyclin D1 promoter activity, correlating with a decrease in cyclin D1 protein and mRNA levels (*39*). Concordantly, in *Ptch1*$^{+/-}$/B6 mice the predicted pathways identified by the deregulated miRNAs converged on the deregulation of cyclin D, making it reasonable that a slow and more robust repair in C57Bl/6J mice might be protective from radiation-induced lens opacity. On the contrary, a fast and less accurate DNA repair in *Ptch1*$^{+/-}$/CD1 lenses can promote basal/mesenchymal transdifferentiation (*40*), which may lead to a radiation-induced EMT-dependent lens opacity.

p53, in fact, functions not only as tumor suppressor and ''guardian of the genome'', and over the past decade the p53 network has been extended to transcriptional regulation of

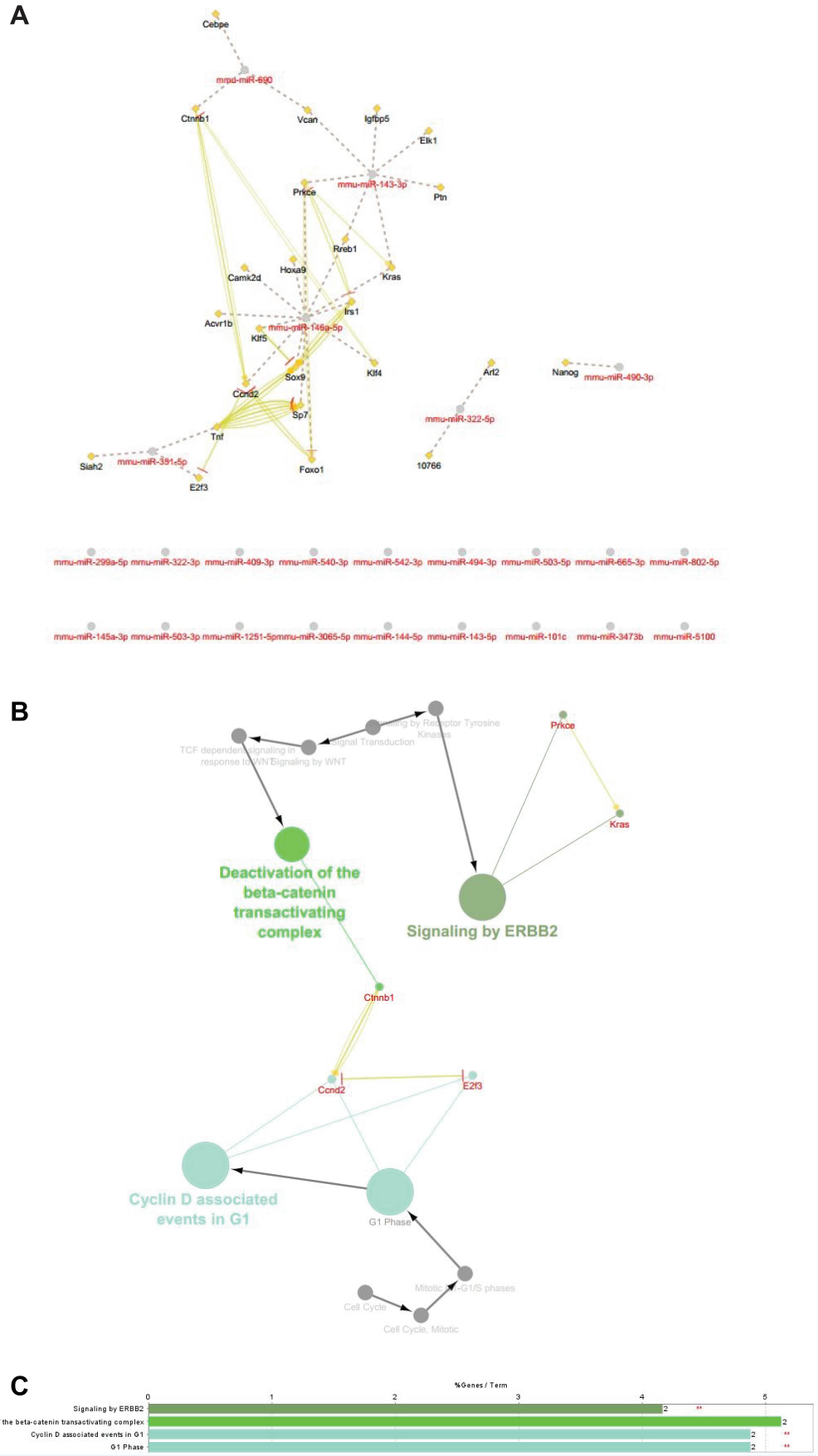

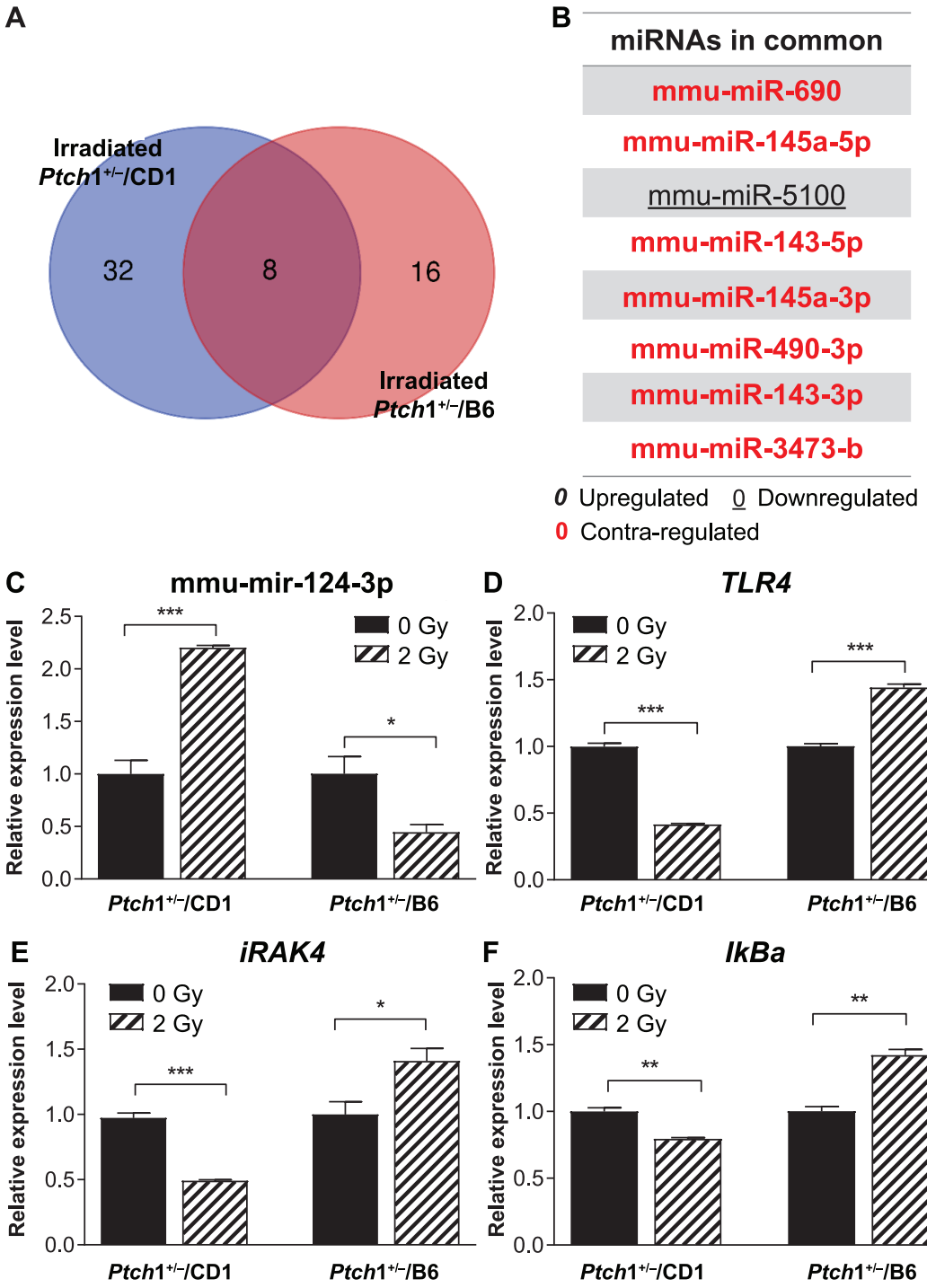

FIG. 3. Intersection between mouse strains. Panel A: Venn diagram showing overlap between the statistically significant miRNAs perturbed in the 2 Gy irradiated *Ptch1*$^{+/-}$/CD1 (left side) and 2 Gy irradiated *Ptch1*$^{+/-}$/B6 mouse lenses (right side). Panel B: Common miRNAs are listed, shown as upregulated (bold face), downregulated (underlined) or contra-regulated (red). Panels C–F: Validation by qPCR analysis of the TLRs cascade deregulation of mmu-miR-124-3p, *TLR4*, *iRAK4* and *IkBa* expression levels, respectively. Each dataset represents the mean ± SEM of three independent biological replicates. *$P \leq 0.05$; **$P \leq 0.01$; ***$P \leq 0.001$.

←

FIG. 2. *Ptch1*$^{+/-}$/B6 mouse lenses: Pathway analysis. Panels A and B: miRNAs and their predicted target genes, and corresponding pathway analysis, respectively. Panel C: Histogram showing the most significant REACTOME pathways associated with the statistically significant miRNAs altered in 2 Gy irradiated vs. nonirradiated *Ptch1*$^{+/-}$/B6 mouse lenses, listed in Table 2.

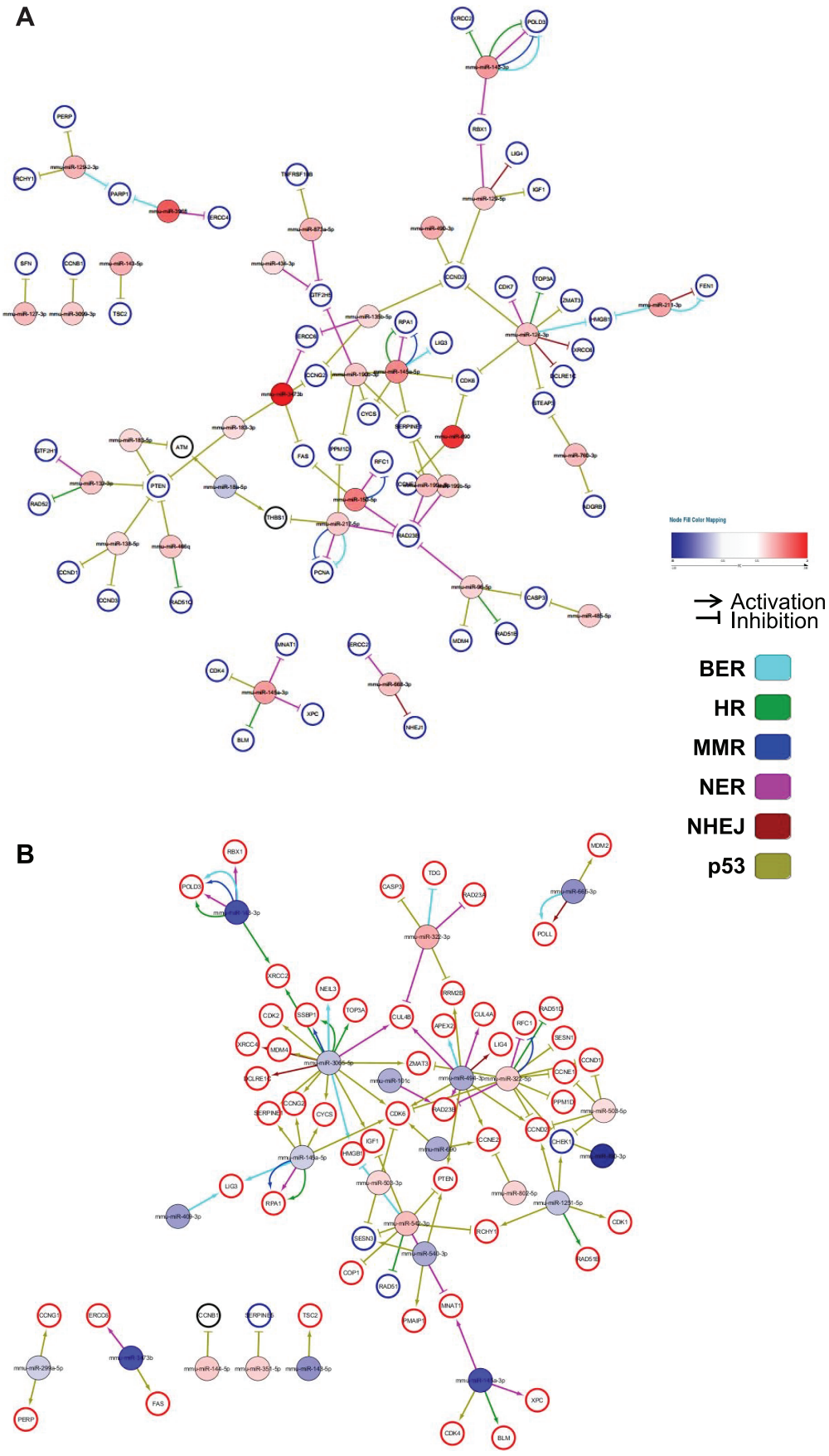

genes associated with a wide variety of biological functions including DNA repair, angiogenesis, cellular metabolism, inflammation, autophagy, stem cell renewal, fertility, differentiation and cellular reprogramming (*41*). Furthermore, p53 has been reported to have a role in TLR expression and most of the TLR genes have been demonstrated to respond to p53 via canonical as well as non-canonical promoter binding sites (*42*).

Tissue injury is reported to cause inflammation through release of damage-associated molecular patterns (DAMPs) which act upon *TLR2*, *TLR4*, and *TLR9*, therefore inducing TLR signaling activation (*43*). Upon recognition of DAMPs, TLRs recruit TIR domain-containing adaptor proteins, which initiate signal transduction pathways culminating in the activation of NF-kB, IRFs or MAP kinases that regulate the expression of cytokines, chemokines and type I IFNs (*44*). Moreover, during injury, the upregulation of TLRs, through the activation of the pro-survival factor NF-kB, may act as a cell-fate counterbalance to the p53-mediated pro-apoptotic responses (*45*). Therefore, the combined activation of p53 and TLR signaling in *Ptch1*$^{+/-}$/B6 lenses shortly after irradiation could result in a protective function, abrogating development of radiation-induced cataract in *Ptch1*$^{+/-}$/B6 mice (results reported in another article included in this special issue). Notably, miRNA enrichment and pathway analysis after irradiation of *Ptch1*$^{+/-}$/B6 lenses (Fig. 2) showed deregulation of cell cycle progression, consistent with the upregulation of p53 signaling and confirmed by upregulation of p21. In support of our interpretation, compelling evidence highlights that the DDR and immune response signaling networks are activated in concert in response to DAMPs, preventing disease development at early stages, while promoting disease progression at later stages (*46*). Of interest, chaperone peptides of α-crystallin inhibit LEC apoptosis, protein insolubilization and lens opacification (*47*) and specific aB-crystallins are novel p53-target genes and required for p53-dependent apoptosis (*48*). Future investigations on chaperones may be useful to sustain the protective role of p53 against lens opacity/cataract development.

Another function of p53 is to restrain the epithelial cell plasticity, which partly occurs by negatively regulating factors that initiate and maintain EMT program. In this respect, the p53-miRNA–EMT-transcription factors axis has constituted a prevailing paradigm that explains p53-dependent epithelial integrity (*49*). Notably, members of the miR-34 family, the most prevalent p53-induced miRNAs (*42*) have also been implicated in the regulation of EMT, migration and invasion. It has been shown that repression of miR-34a is required for TGF-β-induced EMT (*50*), suggesting that miR-34a is a suppressor of EMT. From a mechanistic point of view, it is conceivable that radiation exposure in *Ptch1*$^{+/-}$/B6, through the activation of p53 signaling and consequent upregulation of miR-34a, might suppress EMT, since it was not histologically observed in the lenses from irradiated *Ptch1*$^{+/-}$/B6 mice.

Of interest, in neonatally irradiated lenses from *Ptch1*$^{+/-}$/CD1 mice, we showed a self-amplifying Shh/TGF-β pathogenic loop, underlying the radiation-induced EMT-dependent cataract (*22*). This was accompanied by evasion from apoptosis and proliferation arrest in LECs, suggestive of a nonfunctional p53-p21 axis at the G_1/S checkpoint. The same mechanism may operate in LECs irradiated in adult age, although with a lower induction of cataract/lens opacity due to age-related decrease of proliferation in LECs. Although morphological examination of nonirradiated mouse lenses at 4 months postirradiation produced no difference between *Ptch1*$^{+/-}$/CD1 and *Ptch1*$^{+/-}$/B6 mice, we detected in the irradiated lenses of *Ptch1*$^{+/-}$/CD1 mice the presence of abnormalities in both anterior and posterior poles, as well as the presence of mislocated nuclei at both lens poles and N-cadherin expression in the LECs. E-cadherin loss in epithelial cells indicates, in fact, significant changes in the actin cytoskeleton, resulting in a shift of actin and its regulatory proteins and complexes; these changes are accompanied by the expression of mesenchymal markers such as N-cadherin, vimentin and fibronectin and a change in cell polarity (*51*). This was associated with an increase in Smad3 mRNA and phospho-Smad3 protein levels in *Ptch1*$^{+/-}$/CD1 irradiated lenses, which was not detected in irradiated lenses from *Ptch1*$^{+/-}$/B6 mice, consistent with a TGF-β-induced EMT typically associated to ASC development (*22, 38*). Accordingly, the absence of the self-amplifying Shh/TGF-β pathogenic loop in CD1 mice may explain why no alterations were observed in WT lenses at 4 months after irradiation and, on the other hand, sustains the long-term propensity of irradiated CD1 mice to develop lens opacity, although at a lower extent than irradiated *Ptch1*$^{+/-}$/CD1 mice (results reported in another article included in this special issue).

Radiation is reported to induce expression of TGF-β that is required for DNA repair, cell cycle progression and early inflammatory response, and involved in the pathogenesis of radiation injury such as fibrosis. The intracellular effectors of TGF-β signaling are the Smad proteins (Smad2/3), which

←

FIG. 4. *Ad hoc* analysis of miRNome data to investigate the DDR. Network visualizations show the different activations of DNA repair mechanisms mediated by miRNAs in irradiated *Ptch1*$^{+/-}$/CD1 (panel A) and *Ptch1*$^{+/-}$/B6 (panel B) mouse lenses. Upregulated/downregulated miRNAs are represented by the colored spheres (shades of red and blue, respectively). The colored interconnection arrows between miRNAs and upregulated/downregulated targeted genes (red/blue bordered spheres) represent the DDR pathway involved, according to the six different colors showed in the figure.

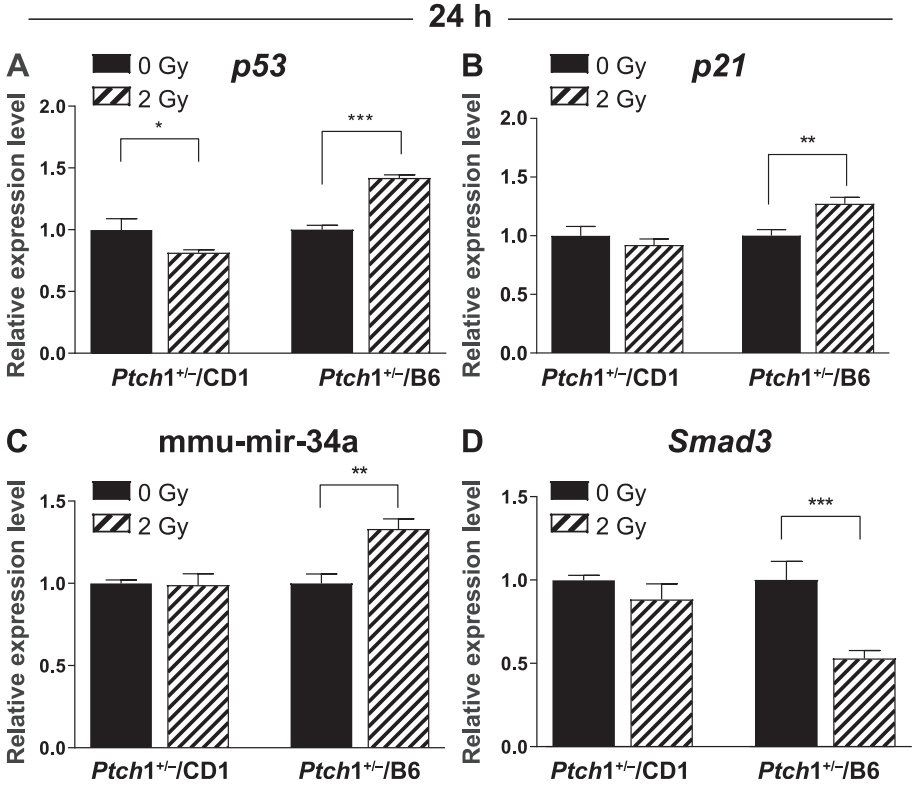

FIG. 5. Correlation between DDR and EMT activation. Evaluation of *p53* (panel A), *p21* (panel B), mmu-miR-34a (panel C) and *Smad3* (panel D) expression levels determined by qPCR analysis in nonirradiated and irradiated *Ptch1*$^{+/-}$/CD1 and *Ptch1*$^{+/-}$/B6 mouse lenses at 24 h postirradiation. Panel E: Evaluation of *Smad3* mRNA expression level determined by qPCR analysis in nonirradiated and irradiated *Ptch1*$^{+/-}$/CD1 and *Ptch1*$^{+/-}$/B6 mouse lenses 4 months postirradiation. Each dataset represents the mean ± SEM of three independent biological replicates. Panels F and G: Expression level of p-Smad3. Western blot analysis of p-Smad3 expression in nonirradiated and irradiated *Ptch1*$^{+/-}$/CD1 and *Ptch1*$^{+/-}$/B6 mouse lenses was performed. Band intensities of p-Smad3 were measured in three independent blots and normalized against β-actin. Panels H–L: Representative images of lens abnormalities revealed in *Ptch1*$^{+/-}$/CD1 mouse 4 months postirradiation. Mislocated nuclei (arrows) in the anterior pole (panel H) and bladder cells in the posterior pole (panels K and L). N-cad immunoreactivity (panel I) and multilayered plaques (arrows) in the anterior and posterior poles, consisting of spindle-shaped cells, typically associated to EMT activation (panel J and L). Scale bars = 10 μm. *$P \leq 0.05$; **$P \leq 0.01$; ***$P \leq 0.001$.

when activated through phosphorylation, translocate into the nucleus, where they regulate transcription (*52*). Of note, miR-34 was shown to downregulate the expression of key genes in TGF-β pathway, such as the TGF-β receptor 1 (TGF-βR1), Smad3 and Smad4 (*53, 54*). Consistent with this, we found increased miR-34a and decreased Smad3 expression levels in *Ptch1*$^{+/-}$/B6 irradiated lenses compared to nonirradiated ones, suggesting that TGF-β-induced EMT can be counteracted by the activation of p53-mediated signaling.

Moreover, miRNome analysis also implied Wnt/β-catenin pathway through the deactivation of the β-catenin trans-activating complex in *Ptch1*$^{+/-}$/B6 irradiated lenses. The Wnt/β-catenin pathway is involved in many cellular processes, such as proliferation, migration, polarization, cellular differentiation and, importantly, cooperates with the TGF-β pathway to induce complete EMT (*55*). Consistent with this, deactivation of the β-catenin and increased miR-34a could act together to counteract TGF-β-induced EMT in irradiated *Ptch1*$^{+/-}$/B6 but not *Ptch1*$^{+/-}$/CD1 lenses, where no differences in the expression of miR-34a, Smad3 and Wnt/β-catenin pathway were detected after irradiation.

In summary, our results demonstrated the existence of important genetic background-related differences in miR-Nome profiles, modulating the expression of genes involved in injury, repair, proliferation and remodeling (EMT) in the mouse lens early after irradiation, which may mechanistically account for differences in susceptibility to radiation-induced cataract in *Ptch1*$^{+/-}$/CD1 and *Ptch1*$^{+/-}$/B6 mice.

SUPPLEMENTARY INFORMATION

Table S1. Optical density and RNA integrity numbers (RIN) measurements for all RNA samples.

Table S2. Primer sequences used for qPCR.

Fig. S1. Predicted pathways obtained from the 55 (51 up- and 4 downregulated) statistically differentially expressed miRNAs ($P < 0.05$) found comparing 2 Gy irradiated to

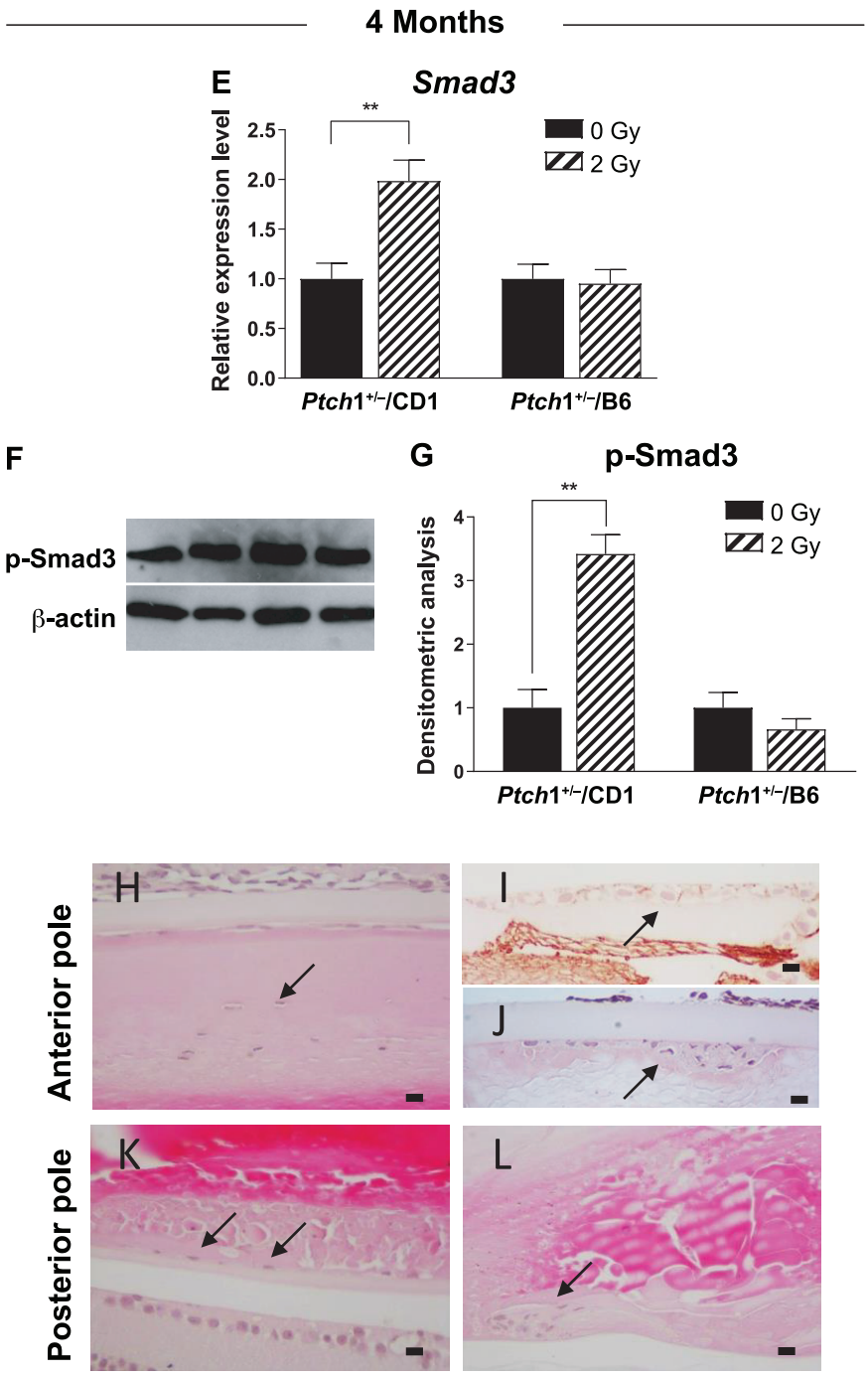

FIG. 5. Continued.

nonirradiated CD1 mouse lenses, clearly showing the activation of almost all pathways listed in Fig. 1C. Alternatively, among the very low number of statistically differentially expressed miRNAs (n = 13, $P < 0.05$, all downregulated) obtained from C57Bl/6J mouse lenses (2 Gy vs. 0 Gy), the only predicted pathway was the mTOR signaling, suggesting again a deregulation of cell cycle progression.

ACKNOWLEDGMENTS

This study was supported by the LDLensRad project that received funding from the Euratom Research and Training Programme 2014–2018, in the framework of the CONCERT EJP (grant agreement no. 662287). This publication reflects only the authors' views. Responsibility for the information and views expressed herein lies entirely with the authors. The European Commission is not responsible for any use that may be made of the information it contains. We are grateful to Dr. Maria Pimpinella and Ms. Vanessa De Coste of the ENEA National Institute of Ionizing

Radiation Metrology (ENEA-INMRI) for their support with irradiation and dosimetry. This work is dedicated to the memory of our friend and colleague Gabriele Babini, who prematurely passed away on November 5, 2020.

Received: November 4, 2020; accepted: March 11, 2021; published online: April 15, 2021

REFERENCES

1. Pritchard CC, Cheng HH, Tewari M. MicroRNA profiling: approaches and considerations. Nat Rev Genet 2012; 13:358–69.
2. Flynt AS, Lai EC. Biological principles of microRNA-mediated regulation: shared themes amid diversity. Nat Rev Genet 2008; 9:831–42.
3. Huang HY, Lin YC, Li J, Huang KY, Shrestha S, Hong HC, et al. miRTarBase 2020: updates to the experimentally validated microRNA-target interaction database. Nucleic Acids Res 2020; 48:D148-D54.
4. Weige T, Liu B, Qu S, Liang G, Luo W, Gong C. MicroRNAs and cancer: Key paradigms in molecular therapy. Oncol Lett 2018; 15: 2735–42.
5. Saheli S, Sathyamoorthy B, Sheeja R, Urmi P, Anuradha D, Buddhadeb D, et al. MicroRNA: A new therapeutic strategy for cardiovascular diseases. Trends Cardiovasc Med 2016; 26: 407–19.
6. Neudecker V, Yuan X, Bowser JL, Eltzschig HK. MicroRNAs in mucosal inflammation. J Mol Med (Berl) 2017; 95:935–49.
7. Salvi V, Gianello V, Tiberio L, Sozzani S, Bosisio D. Cytokine targeting by miRNAs in autoimmune diseases. Front Immunol 2019; 10:15.
8. Szabo G, Bala S. MicroRNAs in liver disease. Nat Rev Gastroenterol Hepatol 2013; 10:542–52.
9. Babalola O, Mamalis A, Lev-Tov H, Jagdeo J. The role of microRNAs in skin fibrosis. Arch Dermatol Res 2013; 305:763–76.
10. Nadim WD, Simion V, Benedetti H, Pichon C, Baril P, Morisset-Lopez S. MicroRNAs in neurocognitive dysfunctions: New molecular targets for pharmacological treatments? Curr Neuropharmacol 2017; 15:260–75.
11. Yu X, Zheng H, Chan MT, Wu WKK. MicroRNAs: new players in cataract. Am J Transl Res 2017; 9:3896–903.
12. Wu C, Lin H, Wang Q, Chen W, Luo H, Zhang H. Discrepant expression of microRNAs in transparent and cataractous human lenses. Invest Ophthalmol Vis Sci 2012; 53:3906–12.
13. Wu C, Liu Z, Ma L, Pei C, Qin L, Gao N, et al. MiRNAs regulate oxidative stress related genes via binding to the 3′ UTR and TATA-box regions: a new hypothesis for cataract pathogenesis. BMC Ophthalmol 2017; 17:142.
14. Valko M, Leibfritz D, Moncol J, Cronin MTD, Mazur M, Telser J. Free radicals and antioxidants in normal physiological functions and human disease. Int J Biochem Cell Biol 2007; 39:44–84.
15. Robman L, Taylor H. External factors in the development of cataract. Eye (Lond) 2005; 19:1074–82.
16. Stewart FA, Akleyev AV, Hauer-Jensen M, Hendry JH, Kleiman NJ, Macvittie TJ, et al. ICRP publication 118: ICRP statement on tissue reactions and early and late effects of radiation in normal tissues and organs–threshold doses for tissue reactions in a radiation protection context. Ann ICRP 2012; 41:1–322.
17. Hamada N, Azizova TV, Little MP. An update on effects of ionizing radiation exposure on the eye. Br J Radiol 2020; 93:20190829.
18. Ainsbury EA, Dalke C, Hamada N, Benadjaoud MA, Chumak V, Ginjaume M, et al. Radiation-induced lens opacities: Epidemiological, clinical and experimental evidence, methodological issues, research gaps and strategy. Environ Int 2021; 146:106213.
19. Ainsbury EA, Barnard S, Bright S, Dalke C, Jarrin M, Kunze S, et al. Ionizing radiation induced cataracts: Recent biological and mechanistic developments and perspectives for future research. Mutat Res 2016; 770(Pt B):238–61.
20. Worgul BV, Smilenov L, Brenner DJ, Junk A, Zhou W, Hall EJ. Atm heterozygous mice are more sensitive to radiation-induced cataracts than are their wild-type counterparts Proc Natl Acad Sci U S A 2002; 99:9836–9.
21. Kleiman NJ, David J, Elliston CD, Hopkins KM, Smilenov LB, Brenner DJ, et al. Mrad9 and atm haploinsufficiency enhance spontaneous and X-ray-induced cataractogenesis in mice. Radiat Res 2007; 168:567–73.
22. De Stefano I, Tanno B, Giardullo P, Leonardi S, Pasquali E, Antonelli F, et al. The Patched 1 tumor-suppressor gene protects the mouse lens from spontaneous and radiation-induced cataract. Am J Pathol 2015; 185:85–95.
23. Sakashita T, Sato T, Hamada N. A biologically based mathematical model for spontaneous and ionizing radiation cataractogenesis. PLoS One 2019; 14:e0221579.
24. Barakat MT, Humke EW, Scott MP: Learning from Jekyll to control Hyde: Hedgehog signaling in development and cancer. Trends Mol Med 2010; 16:337–48.
25. Kerr CL, Huang J, Williams T, West-Mays JA. Activation of the hedgehog signaling pathway in the developing lens stimulates ectopic FoxE3 expression and disruption in fiber cell differentiation. Invest Ophthalmol Vis Sci 2012; 53:3316–30.
26. De Stefano I, Giardullo P, Tanno B, Leonardi S, Pasquali E, Babini G, et al. Nonlinear radiation-induced cataract using the radiosensitive Ptch1(+/–) mouse model. Radiat Res 2016; 186:315–21.
27. Hahn H, Wojnowski L, Zimmer AM, Hall J, Miller G, Zimmer A. Rhabdomyosarcomas and radiation hypersensitivity in a mouse model of Gorlin syndrome. Nat Med 1998; 4:619–22.
28. Tanno B, Babini G, Leonardi S, Giardullo P, De Stefano I, Pasquali E, et al. Ex vivo miRNome analysis in Ptch1+/– cerebellum granule cells reveals a subset of miRNAs involved in radiation-induced medulloblastoma. Oncotarget 2016; 7:68253–69.
29. Bindea G, Galon J, Mlecnik B. CluePedia Cytoscape plugin: Pathway insights using integrated experimental and in silico data. Bioinformatics 2013; 29:661–3.
30. Singh BP, Chauhan RS, Lokesh K. Singhal LK. Toll-like receptors and their role in innate immunity. Curr Sci 2003; 85:1156–64.
31. Baldin V, Lukas J, Marcote MJ, Pagano M, Draetta G. Cyclin D1 is a nuclear protein required for cell cycle progression in G1. Genes Dev 1993; 7:812–21.
32. He X, Jing Z1, Cheng G. MicroRNAs: new regulators of Toll-like receptor signalling pathways. Biomed Res Int 2014; 2014:945169.
33. Ma C, Li Y, Li M, Deng G, Wu X, Zeng J, et al. microRNA-124 negatively regulates TLR signaling in alveolar macrophages in response to mycobacterial infection. Mol Immunol 2014; 62:150–8.
34. He L, He X, Lim LP, de Stanchina E, Xuan Z, Liang Y, et al. A microRNA component of the p53 tumour suppressor network. Nature 2007; 447:1130–4.
35. Zhang L, Liao Y, Tang L. MicroRNA-34 family: a potential tumor suppressor and therapeutic candidate in cancer. J Exp Clin Cancer Res 2019; 38:53.
36. Dancea HC, Shareef MM, Ahmed MM. Role of radiation-induced TGF-beta signaling in cancer therapy. Mol Cell Pharmacol 2009; 1:44–56.
37. Clayton SW, Ban GI, Liu C, Serra R. Canonical and noncanonical TGF-beta signaling regulate fibrous tissue differentiation in the axial skeleton. Sci Rep. 2020; 10:21364.
38. Lovicu FJ, Ang S, Chorazyczewska M, McAvoy JW. Deregulation of lens epithelial cell proliferation and differentiation during the development of TGFbeta-induced anterior subcapsular cataract. Dev Neurosci 2004; 26:446–55.
39. Rocha S, Martin AM, Meek DW, Perkins ND. p53 represses cyclin D1 transcription through down regulation of Bcl-3 and inducing

increased association of the p52 NF-kappaB subunit with histone deacetylase 1. Mol Cell Biol 2003; 23:4713–27.

40. Wang H, Xiang D, Liu B, He A, Randle HJ, Zhang KX, et al. Inadequate DNA damage repair promotes mammary transdifferentiation, leading to BRCA1 breast cancer. Cell 2019; 178:135–51.

41. Jain AK, Barton MC. p53: emerging roles in stem cells, development and beyond. Development 2018; 145:dev158360.

42. Menendez D, Shatz M, Azzam K, Garantziotis S, Fessler MB, Resnick MA. The Toll-like receptor gene family is integrated into human DNA damage and p53 networks. PLoS Genet 2011; 7:e1001360.

43. Piccinini AM, Midwood KS. DAMPening inflammation by modulating TLR Signalling. Mediators Inflamm 2010; 2010:672395.

44. Kawasaki T, Kawai T. Toll-like receptor signaling pathways. Front Immunol 2014; 5:461.

45. Jiang D, Liang J, Fan J, Yu S, Chen S, Luo Y, et al. Regulation of lung injury and repair by Toll-like receptors and hyaluronan. Nat Med 2005; 11:1173–9.

46. Pateras IS, Havaki S, Nikitopoulou X, Vougas K, Townsend PA, Panayiotidis MI, et al. The DNA damage response and immune signaling alliance: Is it good or bad? Nature decides when and where. Pharmacol Ther 2015; 154:36–56.

47. Nahomi RB, Wang B, Raghavan CT, Voss O, Doseff AI, Santhoshkumar P, et al. Chaperone peptides of α-crystallin inhibit epithelial cell apoptosis, protein insolubilization, and opacification in experimental cataracts. J Biol Chem 2013; 288:13022–35.

48. Watanabe G, Kato S, Nakata H, Ishida T, Ohuchi N, Ishioka C. alphaB-crystallin: a novel p53-target gene required for p53-dependent apoptosis. Cancer Sci 2009; 100:2368–75.

49. Puisieux A, Brabletz T, Caramel J. Oncogenic roles of EMT-inducing transcription factors. Nat Cell Biol 2014; 16:488–94.

50. Bommer GT, Gerin I, Feng Y, Kaczorowski AJ, Kuick R, Love RE, et al. p53-mediated activation of miRNA34 candidate tumor-suppressor genes. Curr Biol 2007; 17:1298–307.

51. Morris HT, Machesky LM. Actin cytoskeletal control during epithelial to mesenchymal transition: focus on the pancreas and intestinal tract. Br J Cancer 2015; 112:613–20.

52. Wrana JL, Attisano L, Wieser R, Ventura F, Massague J. Mechanism of activation of the TGF-beta receptor. Nature 1994; 370:341–7.

53. Du R, Sun W, Xia L, Zhao A, Yu Y, Zhao L, et al. Hypoxia-induced down-regulation of microRNA-34a promotes EMT by targeting the Notch signaling pathway in tubular epithelial cells. PLoS One 2012; 7:e30771.

54. Fang LL, Sun BF, Huang LR, Yuan HB, Zhang S, Chen J, et al. Potent inhibition of miR-34b on migration and invasion in metastatic prostate cancer cells by regulating the TGF-beta pathway. Int J Mol Sci 2017; 18:2762.

55. Fuxe J, Vincent T, Garcia de Herreros A. Transcriptional crosstalk between TGF-beta and stem cell pathways in tumor cell invasion: role of EMT promoting Smad complexes. Cell Cycle 2010; 9:2363–74.